The Ratio of Isolated Photon Cross Sections at $\sqrt{s} = 630$ GeV and 1800 GeV

V.M. Abazov,[23] B. Abbott,[58] A. Abdesselam,[11] M. Abolins,[51] V. Abramov,[26] B.S. Acharya,[17] D.L. Adams,[60] M. Adams,[38] S.N. Ahmed,[21] G.D. Alexeev,[23] G.A. Alves,[2] N. Amos,[50] E.W. Anderson,[43] Y. Arnoud,[9] M.M. Baarmand,[55] V.V. Babintsev,[26] L. Babukhadia,[55] T.C. Bacon,[28] A. Baden,[47] B. Baldin,[37] P.W. Balm,[20] S. Banerjee,[17] E. Barberis,[30] P. Baringer,[44] J. Barreto,[2] J.F. Bartlett,[37] U. Bassler,[12] D. Bauer,[28] A. Bean,[44] F. Beaudette,[11] M. Begel,[54] A. Belyaev,[35] S.B. Beri,[15] G. Bernardi,[12] I. Bertram,[27] A. Besson,[9] R. Beuselinck,[28] V.A. Bezzubov,[26] P.C. Bhat,[37] V. Bhatnagar,[11] M. Bhattacharjee,[55] G. Blazey,[39] S. Blessing,[35] A. Boehnlein,[37] N.I. Bojko,[26] F. Borcherding,[37] K. Bos,[20] A. Brandt,[60] R. Breedon,[31] G. Briskin,[59] R. Brock,[51] G. Brooijmans,[37] A. Bross,[37] D. Buchholz,[40] M. Buehler,[38] V. Buescher,[14] V.S. Burtovoi,[26] J.M. Butler,[48] F. Canelli,[54] W. Carvalho,[3] D. Casey,[51] Z. Casilum,[55] H. Castilla-Valdez,[19] D. Chakraborty,[39] K.M. Chan,[54] S.V. Chekulaev,[26] D.K. Cho,[54] S. Choi,[34] S. Chopra,[56] J.H. Christenson,[37] M. Chung,[38] D. Claes,[52] A.R. Clark,[30] J. Cochran,[34] L. Coney,[42] B. Connolly,[35] W.E. Cooper,[37] D. Coppage,[44] S. Crépé-Renaudin,[9] M.A.C. Cummings,[39] D. Cutts,[59] G.A. Davis,[54] K. Davis,[29] K. De,[60] S.J. de Jong,[21] K. Del Signore,[50] M. Demarteau,[37] R. Demina,[45] P. Demine,[9] D. Denisov,[37] S.P. Denisov,[26] S. Desai,[55] H.T. Diehl,[37] M. Diesburg,[37] S. Doulas,[49] Y. Ducros,[13] L.V. Dudko,[25] S. Duensing,[21] L. Duflot,[11] S.R. Dugad,[17] A. Duperrin,[10] A. Dyshkant,[39] D. Edmunds,[51] J. Ellison,[34] V.D. Elvira,[37] R. Engelmann,[55] S. Eno,[47] G. Eppley,[62] P. Ermolov,[25] O.V. Eroshin,[26] J. Estrada,[54] H. Evans,[53] V.N. Evdokimov,[26] T. Fahland,[33] S. Feher,[37] D. Fein,[29] T. Ferbel,[54] F. Filthaut,[21] H.E. Fisk,[37] Y. Fisyak,[56] E. Flattum,[37] F. Fleuret,[30] M. Fortner,[39] H. Fox,[40] K.C. Frame,[51] S. Fu,[53] S. Fuess,[37] E. Gallas,[37] A.N. Galyaev,[26] M. Gao,[53] V. Gavrilov,[24] R.J. Genik II,[27] K. Genser,[37] C.E. Gerber,[38] Y. Gershtein,[59] R. Gilmartin,[35] G. Ginther,[54] B. Gómez,[5] G. Gómez,[47] P.I. Goncharov,[26] J.L. González Solís,[19] H. Gordon,[56] L.T. Goss,[61] K. Gounder,[37] A. Goussiou,[28] N. Graf,[56] G. Graham,[47] P.D. Grannis,[55] J.A. Green,[43] H. Greenlee,[37] Z.D. Greenwood,[46] S. Grinstein,[1] L. Groer,[53] S. Grünendahl,[37] A. Gupta,[17] S.N. Gurzhiev,[26] G. Gutierrez,[37] P. Gutierrez,[58] N.J. Hadley,[47] H. Haggerty,[37] S. Hagopian,[35] V. Hagopian,[35] R.E. Hall,[32] P. Hanlet,[49] S. Hansen,[37] J.M. Hauptman,[43] C. Hays,[53] C. Hebert,[44] D. Hedin,[39] J.M. Heinmiller,[38] A.P. Heinson,[34] U. Heintz,[48] T. Heuring,[35] M.D. Hildreth,[42] R. Hirosky,[63] J.D. Hobbs,[55] B. Hoeneisen,[8] Y. Huang,[50] R. Illingworth,[28] A.S. Ito,[37] M. Jaffré,[11] S. Jain,[17] R. Jesik,[28] K. Johns,[29] M. Johnson,[37] A. Jonckheere,[37] M. Jones,[36] H. Jöstlein,[37] A. Juste,[37] W. Kahl,[45] S. Kahn,[56] E. Kajfasz,[10] A.M. Kalinin,[23] D. Karmanov,[25] D. Karmgard,[42] Z. Ke,[4] R. Kehoe,[51] A. Khanov,[45] A. Kharchilava,[42] S.K. Kim,[18] B. Klima,[37] B. Knuteson,[30] W. Ko,[31] J.M. Kohli,[15] A.V. Kostritskiy,[26] J. Kotcher,[56] B. Kothari,[53] A.V. Kotwal,[53] A.V. Kozelov,[26] E.A. Kozlovsky,[26] J. Krane,[43] M.R. Krishnaswamy,[17] P. Krivkova,[6] S. Krzywdzinski,[37] M. Kubantsev,[45] S. Kuleshov,[24] Y. Kulik,[55] S. Kunori,[47] A. Kupco,[7] V.E. Kuznetsov,[34] G. Landsberg,[59] W.M. Lee,[35] A. Leflat,[25] C. Leggett,[30] F. Lehner,[37,*] J. Li,[60] Q.Z. Li,[37] X. Li,[4] J.G.R. Lima,[3] D. Lincoln,[37] S.L. Linn,[35] J. Linnemann,[51] R. Lipton,[37] A. Lucotte,[9] L. Lueking,[37] C. Lundstedt,[52] C. Luo,[41] A.K.A. Maciel,[39] R.J. Madaras,[30] V.L. Malyshev,[23] V. Manankov,[25] H.S. Mao,[4] T. Marshall,[41] M.I. Martin,[39] K.M. Mauritz,[43] B. May,[40] A.A. Mayorov,[41] R. McCarthy,[55] T. McMahon,[57] H.L. Melanson,[37] M. Merkin,[25] K.W. Merritt,[37] C. Miao,[59] H. Miettinen,[62] D. Mihalcea,[39] C.S. Mishra,[37] N. Mokhov,[37] N.K. Mondal,[17] H.E. Montgomery,[37] R.W. Moore,[51] M. Mostafa,[1] H. da Motta,[2] E. Nagy,[10] F. Nang,[29] M. Narain,[48] V.S. Narasimham,[17] H.A. Neal,[50] J.P. Negret,[5] S. Negroni,[10] T. Nunnemann,[37] D. O'Neil,[51] V. Oguri,[3] B. Olivier,[12] N. Oshima,[37] P. Padley,[62] L.J. Pan,[40] K. Papageorgiou,[38] A. Para,[37] N. Parashar,[49] R. Partridge,[59] N. Parua,[55] M. Paterno,[54] A. Patwa,[55] B. Pawlik,[22] J. Perkins,[60] M. Peters,[36] O. Peters,[20] P. Pétroff,[11] R. Piegaia,[1] B.G. Pope,[51] E. Popkov,[48] H.B. Prosper,[35] S. Protopopescu,[56] J. Qian,[50] R. Raja,[37] S. Rajagopalan,[56] E. Ramberg,[37] P.A. Rapidis,[37] N.W. Reay,[45] S. Reucroft,[49] M. Ridel,[11] M. Rijssenbeek,[55] F. Rizatdinova,[45] T. Rockwell,[51] M. Roco,[37] C. Royon,[13] P. Rubinov,[37] R. Ruchti,[42] J. Rutherfoord,[29] B.M. Sabirov,[23] G. Sajot,[9] A. Santoro,[2] L. Sawyer,[46] R.D. Schamberger,[55] H. Schellman,[40] A. Schwartzman,[1] N. Sen,[62] E. Shabalina,[38] R.K. Shivpuri,[16] D. Shpakov,[49] M. Shupe,[29] R.A. Sidwell,[45] V. Simak,[7] H. Singh,[34] J.B. Singh,[15] V. Sirotenko,[37] P. Slattery,[54] E. Smith,[58] R.P. Smith,[37] R. Snihur,[40] G.R. Snow,[52] J. Snow,[57] S. Snyder,[56] J. Solomon,[38] V. Sorín,[1] M. Sosebee,[60] N. Sotnikova,[25] K. Soustruznik,[6] M. Souza,[2] N.R. Stanton,[45] G. Steinbrück,[53] R.W. Stephens,[60] F. Stichelbaut,[56] D. Stoker,[33] V. Stolin,[24] A. Stone,[46] D.A. Stoyanova,[26] M. Strauss,[58] M. Strovink,[30] L. Stutte,[37] A. Sznajder,[3] M. Talby,[10] W. Taylor,[55] S. Tentindo-Repond,[35] S.M. Tripathi,[31] T.G. Trippe,[30] A.S. Turcot,[56] P.M. Tuts,[53] V. Vaniev,[26] R. Van Kooten,[41] N. Varelas,[38] L.S. Vertogradov,[23] F. Villeneuve-Seguier,[10] A.A. Volkov,[26] A.P. Vorobiev,[26] H.D. Wahl,[35] H. Wang,[40] Z.-M. Wang,[55] J. Warchol,[42] G. Watts,[64] M. Wayne,[42] H. Weerts,[51] A. White,[60] J.T. White,[61] D. Whiteson,[30] J.A. Wightman,[43] D.A. Wijngaarden,[21] S. Willis,[39] S.J. Wimpenny,[34] J. Womersley,[37] D.R. Wood,[49] Q. Xu,[50] R. Yamada,[37] P. Yamin,[56] T. Yasuda,[37] Y.A. Yatsunenko,[23] K. Yip,[56] S. Youssef,[35] J. Yu,[37] Z. Yu,[40] M. Zanabria,[5] X. Zhang,[58] H. Zheng,[42] B. Zhou,[50] Z. Zhou,[43] M. Zielinski,[54] D. Zieminska,[41] A. Zieminski,[41] V. Zutshi,[56] E.G. Zverev,[25] and A. Zylberstejn[13]

(DØ Collaboration)

[1] *Universidad de Buenos Aires, Buenos Aires, Argentina*
[2] *LAFEX, Centro Brasileiro de Pesquisas Físicas, Rio de Janeiro, Brazil*
[3] *Universidade do Estado do Rio de Janeiro, Rio de Janeiro, Brazil*
[4] *Institute of High Energy Physics, Beijing, People's Republic of China*
[5] *Universidad de los Andes, Bogotá, Colombia*
[6] *Charles University, Center for Particle Physics, Prague, Czech Republic*
[7] *Institute of Physics, Academy of Sciences, Center for Particle Physics, Prague, Czech Republic*
[8] *Universidad San Francisco de Quito, Quito, Ecuador*
[9] *Institut des Sciences Nucléaires, IN2P3-CNRS, Universite de Grenoble 1, Grenoble, France*
[10] *CPPM, IN2P3-CNRS, Université de la Méditerranée, Marseille, France*
[11] *Laboratoire de l'Accélérateur Linéaire, IN2P3-CNRS, Orsay, France*
[12] *LPNHE, Universités Paris VI and VII, IN2P3-CNRS, Paris, France*
[13] *DAPNIA/Service de Physique des Particules, CEA, Saclay, France*
[14] *Universität Mainz, Institut für Physik, Mainz, Germany*
[15] *Panjab University, Chandigarh, India*
[16] *Delhi University, Delhi, India*
[17] *Tata Institute of Fundamental Research, Mumbai, India*
[18] *Seoul National University, Seoul, Korea*
[19] *CINVESTAV, Mexico City, Mexico*
[20] *FOM-Institute NIKHEF and University of Amsterdam/NIKHEF, Amsterdam, The Netherlands*
[21] *University of Nijmegen/NIKHEF, Nijmegen, The Netherlands*
[22] *Institute of Nuclear Physics, Kraków, Poland*
[23] *Joint Institute for Nuclear Research, Dubna, Russia*
[24] *Institute for Theoretical and Experimental Physics, Moscow, Russia*
[25] *Moscow State University, Moscow, Russia*
[26] *Institute for High Energy Physics, Protvino, Russia*
[27] *Lancaster University, Lancaster, United Kingdom*
[28] *Imperial College, London, United Kingdom*
[29] *University of Arizona, Tucson, Arizona 85721*
[30] *Lawrence Berkeley National Laboratory and University of California, Berkeley, California 94720*
[31] *University of California, Davis, California 95616*
[32] *California State University, Fresno, California 93740*
[33] *University of California, Irvine, California 92697*
[34] *University of California, Riverside, California 92521*
[35] *Florida State University, Tallahassee, Florida 32306*
[36] *University of Hawaii, Honolulu, Hawaii 96822*
[37] *Fermi National Accelerator Laboratory, Batavia, Illinois 60510*
[38] *University of Illinois at Chicago, Chicago, Illinois 60607*
[39] *Northern Illinois University, DeKalb, Illinois 60115*
[40] *Northwestern University, Evanston, Illinois 60208*
[41] *Indiana University, Bloomington, Indiana 47405*
[42] *University of Notre Dame, Notre Dame, Indiana 46556*
[43] *Iowa State University, Ames, Iowa 50011*
[44] *University of Kansas, Lawrence, Kansas 66045*
[45] *Kansas State University, Manhattan, Kansas 66506*
[46] *Louisiana Tech University, Ruston, Louisiana 71272*
[47] *University of Maryland, College Park, Maryland 20742*
[48] *Boston University, Boston, Massachusetts 02215*
[49] *Northeastern University, Boston, Massachusetts 02115*
[50] *University of Michigan, Ann Arbor, Michigan 48109*
[51] *Michigan State University, East Lansing, Michigan 48824*
[52] *University of Nebraska, Lincoln, Nebraska 68588*
[53] *Columbia University, New York, New York 10027*
[54] *University of Rochester, Rochester, New York 14627*
[55] *State University of New York, Stony Brook, New York 11794*
[56] *Brookhaven National Laboratory, Upton, New York 11973*
[57] *Langston University, Langston, Oklahoma 73050*
[58] *University of Oklahoma, Norman, Oklahoma 73019*
[59] *Brown University, Providence, Rhode Island 02912*

[60] *University of Texas, Arlington, Texas 76019*
[61] *Texas A&M University, College Station, Texas 77843*
[62] *Rice University, Houston, Texas 77005*
[63] *University of Virginia, Charlottesville, Virginia 22901*
[64] *University of Washington, Seattle, Washington 98195*
(28 July 2001)

The inclusive cross section for production of isolated photons has been measured in $p\bar{p}$ collisions at $\sqrt{s} = 630$ GeV with the DØ detector at the Fermilab Tevatron Collider. The photons span a transverse energy (E_T) range from 7–49 GeV and have pseudorapidity $|\eta| < 2.5$. This measurement is combined with the previous DØ result at $\sqrt{s} = 1800$ GeV to form a ratio of the cross sections. Comparison of next-to-leading-order QCD with the measured cross section at 630 GeV and ratio of cross sections show satisfactory agreement in most of the E_T range. While the measured cross section at 630 GeV exceeds the QCD prediction at low E_T, this excess has marginal statistical significance.

13.85.Qk, 12.38.Qk

DRAFT

Photons produced directly from parton-parton interactions provide a powerful and effective means to study the constituents of hadronic matter. Because the primary production mechanism for modest E_T photons at the Fermilab Tevatron is gluon Compton scattering ($qg \to \gamma q$), the cross section for direct-photon production is sensitive to the gluon distribution in the proton [1]. A measurement of the final state photons provides a probe of Quantum Chromodynamics (QCD) without additional complications from fragmentation and jet identification.

Previous experiments, at center-of-mass energies of both 630 GeV [2] and 1800 GeV [3,4], have reported photon production in excess of next-to-leading-order (NLO) QCD predictions at low transverse energies ($E_T^\gamma \lesssim 30$ GeV). This disagreement with data could result from gluon radiation not included in NLO calculations [5] or because the parton distributions are not well known [6].

In this Letter, we present a measurement of the isolated direct-photon cross section in $p\bar{p}$ collisions for photons in two pseudorapidity regions, $|\eta| < 0.9$ and $1.6 < |\eta| < 2.5$, where $\eta = -\ln\tan\frac{\theta}{2}$ and θ is the polar angle with respect to the proton beam. We compare the production cross section at $\sqrt{s} = 630$ GeV with our previously published results at $\sqrt{s} = 1800$ GeV [3]. A ratio of the cross sections at different energies reduces systematic uncertainties and minimizes the sensitivity to the choice of parton distribution functions (PDF) because the measurements at both energies use the same detector and the same analysis method.

In the simple parton model, the dimensionless cross section $E_T^4 \cdot E\frac{d^3\sigma}{d^3p}$, as a function of $x_T = \frac{2E_T}{\sqrt{s}}$, is independent of $\sqrt{s}$. Although deviations from such naive scaling are expected, the dimensionless cross section provides a useful context for comparison with QCD.

The cross section measurement at 630 GeV uses a sample of 520 nb^{-1} of data recorded in 1995 [7] with the DØ detector at the Fermilab Tevatron [8]. The analysis uses the uranium/liquid argon calorimeter to identify electromagnetic (EM) showers, and the drift chambers in front of the calorimeter to differentiate photon showers from electron showers. The EM calorimeter provides full azimuthal (ϕ) coverage, and consists of a central cryostat (CC) with $|\eta| \lesssim 1.1$, and two forward cryostats (EC) with $1.4 \lesssim |\eta| \lesssim 4.0$. The EM calorimeter is divided into four longitudinal layers, EM1–EM4, of approximately 2, 2, 7, and 10 radiation lengths, respectively. Layers EM1, EM2, and EM4 are transversely segmented into projective towers subtending $\Delta\phi \times \Delta\eta = 0.1 \times 0.1$ while EM3 is segmented into 0.05×0.05 sections. The EM energy resolution in the central and forward calorimeter is given by $\sigma_E/E = \{15\%/\sqrt{E(\mathrm{GeV})}\} \oplus 0.3\%$.

Photons interacting in the calorimeter are detected using a three-level triggering system. The first level consists of scintillation counters near the beam pipe, which detect inelastic $p\bar{p}$ collisions. The second level requires a minimum energy deposition in a $\Delta\phi \times \Delta\eta = 0.2 \times 0.2$ trigger tower, with trigger thresholds of 2.0, 3.0, and 7.0 GeV. In the final step, calorimeter clusters are formed with thresholds of 4.5, 8.0, and 14.0 GeV, respectively. The trigger efficiency for photons with energies near threshold is determined for the two highest energy triggers by taking the ratio of events passing the 14.0 (8.0) GeV trigger to those passing the 8.0 (4.5) GeV trigger in an energy regime where the lower energy trigger is 100% efficient. Monte Carlo studies of the trigger algorithms show agreement with the data for the two higher energy triggers, and are used to determine the trigger efficiency for the lowest energy trigger. Trigger efficiencies are typically about 20% at the nominal energy threshold and rise to almost 100% a few GeV above the threshold value. Consequently, photon candidates are accepted only for transverse energies of at least 7.35, 10, and 16 GeV for the three triggers, respectively.

Photon candidates are identified as energy clusters located well within the pseudorapidity boundaries of the central calorimeter ($|\eta| < 0.9$) or the forward calorimeter ($1.6 < |\eta| < 2.5$), and, in the central calorimeter, located at least 1.6 cm from the azimuthal section boundaries. The event vertex position is required to be within 50 cm of the center of the detector. The resulting geometric acceptance is $A = 0.622 \pm 0.007$ (0.787 ± 0.007) in the central (forward) region.

Photon candidates within the acceptance region must satisfy four selection criteria. The showers are required to have shapes consistent with that of single EM showers, as determined in studies using test beams of charged pions and electrons. The shower is required to have more than 96% of its energy deposited in the EM section of the calorimeter. The total transverse energy around any cluster forming a photon candidate must satisfy an isolation requirement $E_T^{\mathcal{R}\le 0.4} - E_T^{\mathcal{R}\le 0.2} < 2.0$ GeV, where $\mathcal{R} = \sqrt{(\Delta\eta)^2 + (\Delta\phi)^2}$ is the distance from the cluster center. The efficiency for these three selection criteria, ϵ_s, is estimated as a function of E_T^γ from a GEANT-based Monte Carlo simulation of the DØ detector. We find $\epsilon_s \sim 60\%$ (75%) in the CC (EC) at 8.0 GeV and $\epsilon_s \sim 88\%$ (90%) above 20 GeV. To minimize background from electrons, photon candidates are rejected if any tracks in the drift chamber extrapolate to within a road of width $\Delta\phi \times \Delta\theta = 0.2 \times 0.2$ defined by the angle subtended by the candidate photon cluster and the initial interaction vertex. This criterion can also discard photon candidates that convert in the material in front of the calorimeter, or that have additional tracks in the road due to charged particles from the underlying event. This selection efficiency and the efficiency for reconstructing tracks are estimated by studying electrons from $Z \to e^+e^-$ events. The total charged tracking efficiency is measured to be 0.858 ± 0.013 (0.593 ± 0.079) in the central (forward) region.

The predominant background to direct photon production arises from the decay of π^0 or η mesons to two photons. The fraction of direct photons is determined from the energy (E_1) deposited in the innermost longitudinal section of the calorimeter (EM1). Photons have a small probability of showering in the material in front of the calorimeter and, thus, tend to deposit little energy in EM1. Sensitivity to the amount of EM1 energy can be used to distinguish multiple photon background from a single photon signal. We use the function $f(E_1) = \log_{10}[1 + \log_{10}\{1 + E_1(\mathrm{GeV})\}]$ as our discriminant to determine the single photon purity. The expected distributions of this function for signal and background are found from events simulated with the PYTHIA Monte Carlo [9] and overlaid with data acquired using a random trigger to model noise, pileup, and multiple $p\bar{p}$ interactions. Three categories of fully simulated events are generated: those containing photons, and background events with and without charged tracks pointing from the interaction vertex to the EM cluster. The two different background samples are generated so that charged and neutral background fractions can be separately fit to the data, thus minimizing uncertainties from the tracking efficiency and from the model used for jet fragmentation. A systematic uncertainty in modeling jet fragmentation is estimated by varying the multiplicity of neutral mesons in the core of PYTHIA jets by $\pm 10\%$. The detector response is modeled using a detailed GEANT simulation with the energy response in EM1 calibrated to match the data from $W \to e\nu$ events.

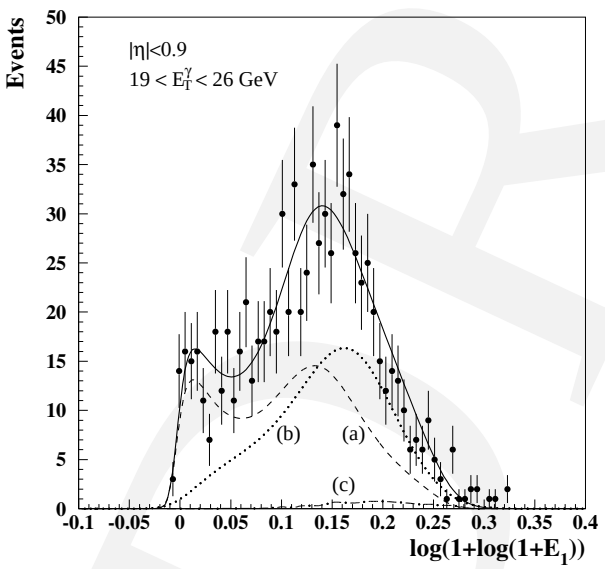

FIG. 1. Distribution of the discriminant for determining photon purity, where E_1 is in units of GeV. Points with error bars indicate data. Broken lines indicate simulated distributions of (a) single photons, and jet background (b) without and (c) with charged tracks. The solid line depicts a fit sum of all three distributions.

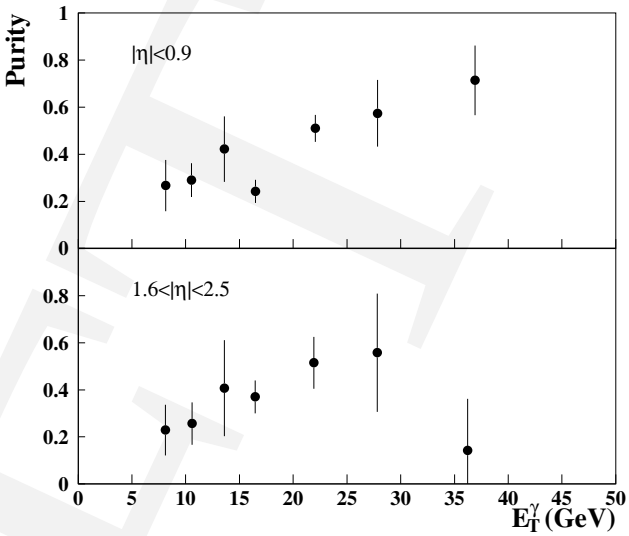

FIG. 2. The photon purity as a function of E_T^γ for central and forward photons. The error bars indicate the uncertainty in the fit purity and are larger than errors derived from statistical analysis alone.

The same criteria used to select photon candidates in the data are applied to the Monte Carlo events. The distribution of f from the data is fitted to a normalized linear combination of Monte Carlo photons and background with and without charged tracks in the road pointing back to the interaction vertex. The fit is performed as a function of E_T^γ using the CERNLIB fitting package HMCMLL [10], with the fractions of signal and background constrained to be between 0.0 and 1.0. The purity is defined as the fraction of Monte Carlo photons in the normalized fitted distribution. A representative fit is shown in Fig. 1 and the photon purity as a function of E_T^γ is plotted in Fig. 2.

The final cross sections $d^2\sigma/dE_T^\gamma d\eta$, after applying efficiency and purity corrections, are shown in Fig. 3 and tabulated in Table I. The error bars show all uncorrelated uncertainties, which include the statistical uncertainty, and uncertainties from selection criteria, trigger efficiency, and the fitted photon purity. The contribution from the fit to photon purity is the largest source of uncorrelated uncertainty. The correlated uncertainty consists of the uncertainties in luminosity, tracking efficiency, geometric acceptance, calorimeter energy scale, and the largest contribution, that from the fragmentation model.

The results are compared with NLO QCD calculations using CTEQ5M [11]. Renormalization and factorization scales of $\mu_R = \mu_F = E_T^{\max}$ are used, where $E_T^{\max}$ is the maximum photon transverse energy in the event. Figure 4 compares the data and theory. A covariance matrix χ^2 provides a measure of the probability that the theory describes the data. A complete covariance matrix, composed of correlated and uncorrelated uncertainties, is de-

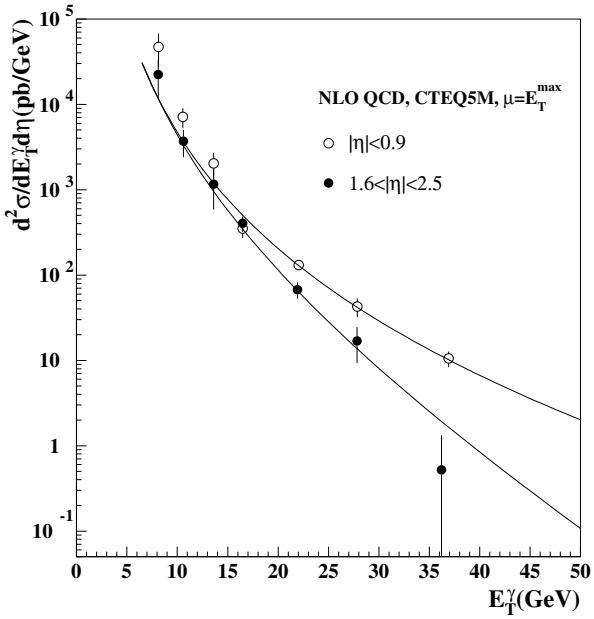

FIG. 3. The cross section for production of isolated photons in central and forward regions at $\sqrt{s} = 630$ GeV. The error bars show the total uncorrelated error, and the curves show cross sections predicted from NLO QCD.

termined and the theoretical cross section is compared to the data with a χ^2 value of 11.4 (4.55) for 7 degrees of freedom in the CC (EC) region. This gives a standard χ^2 probability that the theory is consistent with the data at 12.2% (71.4%) probability in the CC (EC) regions. Deviations between theory and data are largest at low E_T^γ in the central region.

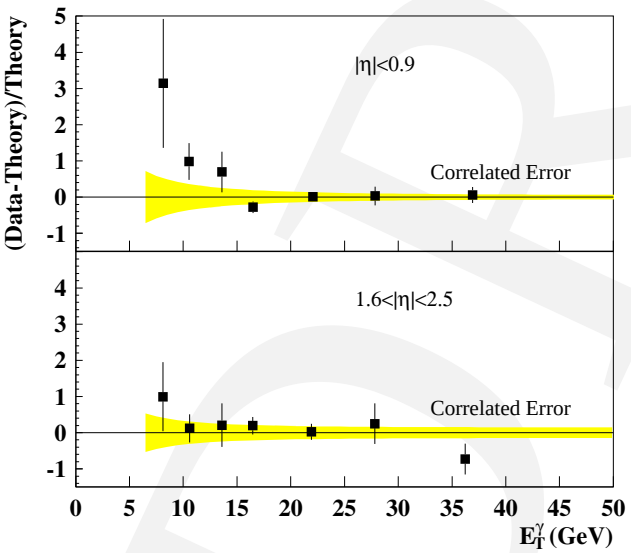

FIG. 4. Comparison of the measured cross section for production of isolated photons at $\sqrt{s} = 630$ GeV with the prediction of NLO QCD using CTEQ5M parton distribution functions.

We combine the cross section reported in this Letter with the DØ measurement at $\sqrt{s} = 1800$ GeV [3]. The cross section at 1800 GeV is increased in every bin by 3.4% from our previously published result to account for the latest value of the proton-antiproton total cross section [13]. The experimental dimensionless cross section, averaged over azimuth, is given by $\sigma_D = \frac{E_T^3}{2\pi} \cdot d^2\sigma/dE_T d\eta$. The ratio of the dimensionless cross sections $\sigma_D(\sqrt{s} = 630\ \text{GeV})/\sigma_D(\sqrt{s} = 1800\ \text{GeV})$, is shown as a function of x_T in Fig. 5 and Table II together with the NLO QCD prediction.

E_T^γ Range (GeV)	Plotted E_T^γ (GeV)	$d^2\sigma/dE_T^\gamma d\eta$ (pb/GeV) NLO QCD	Measured	$\delta\sigma_U$ (%)	$\delta\sigma_C$ (%)
		$\lvert\eta\rvert < 0.9$			
7.35– 9.1	8.2	11400	47000	43	52
9.1–12.6	10.5	3610	7160	26	36
12.6–14.7	13.6	1200	2040	33	25
14.7–18.9	16.5	487	351	22	19
18.9–26.25	22.1	129	131	11	13
26.25–29.75	27.9	41.4	42.6	25	10
29.75–49.0	36.9	9.95	10.5	21	7
		$1.6 < \lvert\eta\rvert < 2.5$			
7.35– 9.1	8.1	11200	22400	48	42
9.1–12.6	10.6	3310	3700	35	31
12.6–14.7	13.6	964	1170	50	24
14.7–18.9	16.5	338	403	20	21
18.9–26.3	21.9	65.4	67.3	22	17
26.25–29.75	27.8	13.6	16.9	45	16
29.75–49.0	36.2	1.91	.522	160	15

TABLE I. The measured and predicted isolated photon production cross section at $\sqrt{s} = 630$ GeV. The value for the column labeled "Plotted E_T^γ" is determined according to Ref. [12]. The columns labeled $\delta\sigma_U$ and $\delta\sigma_C$ are, respectively, the uncorrelated and correlated uncertainties.

Comparison of the theoretical cross section ratio to the data, using the complete covariance matrix, gives a χ^2 value of 6.48 (3.00) for 7 degrees of freedom in the CC (EC), which corresponds to a standard χ^2 probability of 48.5% (88.5%) in the CC (EC) region. Although the lowest x_T points are systematically higher than NLO QCD predictions in both the EC and the CC regions, the deviations are not statistically significant and there exists good agreement between the measured ratio and theory.

We have measured the production cross section for isolated photons in $p\overline{p}$ collisions at $\sqrt{s} = 630$ GeV and compared this cross section with that measured at $\sqrt{s} = 1800$ GeV. Despite some discrepancy between data and the prediction at low E_T, there is good agreement between the data and the theoretical prediction at higher E_T values.

We thank W. Vogelsang and J.F. Owens for their assistance with the theoretical calculations. We thank the staffs at Fermilab and collaborating institutions,

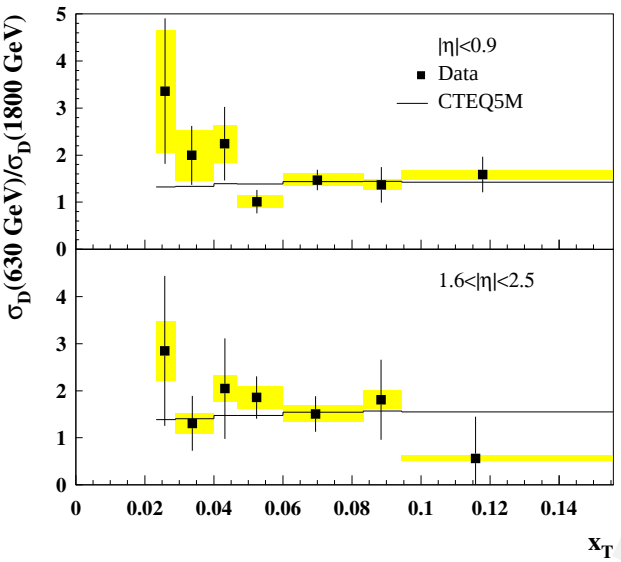

FIG. 5. The ratio of the dimensionless cross sections, $\sigma_D(\sqrt{s} = 630\ \text{GeV})/\sigma_D(\sqrt{s} = 1800\ \text{GeV})$. The error bars indicate the uncorrelated uncertainty and the shaded bands indicate the correlated uncertainty.

and acknowledge support from the Department of Energy and National Science Foundation (USA), Commissariat à L'Energie Atomique and CNRS/Institut National de Physique Nucléaire et de Physique des Particules (France), Ministry for Science and Technology and Ministry for Atomic Energy (Russia), CAPES and CNPq (Brazil), Departments of Atomic Energy and Science and Education (India), Colciencias (Colombia), CONACyT (Mexico), Ministry of Education and KOSEF (Korea), CONICET and UBACyT (Argentina), The Foundation for Fundamental Research on Matter (The Netherlands), PPARC (United Kingdom), Ministry of Education (Czech Republic), and the A.P. Sloan Foundation.

x_T Range	Plotted x_T	Ratio	Theory	$\delta\sigma_U$(%)	$\delta\sigma_C$ (%)
		$\lvert\eta\rvert < 0.9$			
0.023–0.029	0.026	3.36	1.32	46	39
0.029–0.040	0.034	2.00	1.34	31	27
0.040–0.047	0.043	2.24	1.40	35	18
0.047–0.060	0.053	1.01	1.39	25	13
0.060–0.083	0.070	1.47	1.44	15	9
0.083–0.094	0.089	1.37	1.45	27	8
0.094–0.156	0.118	1.59	1.42	23	7
		$1.6 < \lvert\eta\rvert < 2.5$			
0.023–0.029	0.026	2.84	1.39	56	22
0.029–0.040	0.034	1.31	1.41	45	17
0.040–0.047	0.043	2.05	1.47	52	14
0.047–0.060	0.052	1.86	1.48	24	13
0.060–0.083	0.070	1.51	1.54	24	11
0.083–0.094	0.088	1.81	1.57	47	11
0.094–0.156	0.116	0.563	1.55	160	10

TABLE II. The measured ratio and NLO QCD prediction for the dimensionless cross section at $\sqrt{s} = 630$ GeV to that at $\sqrt{s} = 1800$ GeV. The columns labeled $\delta\sigma_U$ and $\delta\sigma_C$ are the uncorrelated and correlated uncertainties, respectively.

* Visitor from University of Zurich, Zurich, Switzerland.

[1] J. Owens, Rev. Mod. Phys. **59**, 465 (1987).
[2] J. Alitti *et al.* (UA2 Collaboration), Phys. Lett. B **263**, 544 (1991); R. Ansari *et al.* (UA2 Collaboration), Z. Phys. C **41**, 395 (1988).
[3] B. Abbott *et al.* (DØ Collaboration) Phys. Rev. Lett. **84**, 2786 (2000).
[4] F. Abe *et al.* (CDF Collaboration), Phys. Rev. Lett. **73**, 2662 (1994); F. Abe *et al.* (CDF Collaboration), Phys. Rev. D **48**, 2998 (1993).
[5] J. Huston *et al.*, Phys. Rev. D **51**, 6139 (1995); H.-L. Lai and H.-N. Li, *ibid.* **58**, 114020 (1998); L. Apanasevich *et al.*, *ibid.* **59**, 074007 (1999).
[6] M. Glück, *et al.*, Phys. Rev. Lett. **73**, 388 (1994); W Giele, in *Proceedings of the 5th International Symposium on Radiative Corrections*, Carmel, CA, September 2000 (to be published electronically at http://www.slac.stanford.edu/econf/).
[7] J. Krane, J. Bantley, and D. Owen, Fermilab-TM-2000, (1997) unpublished.
[8] S. Abachi *et al.* (DØ Collaboration), Nucl. Instrum. Methods Phys. Res. A **338**, 185 (1994).
[9] T. Sjöstrand, Comput. Phys. Commun. **82**, 74 (1995).
[10] R. Barlow and C. Beeston, Comput. Phys. Commun. **77**, 219 (1993).
[11] H. Baer, J. Ohnemus, and J.F. Owens, Phys. Rev. D **42**, 61 (1990); W. Vogelsang and A. Vogt, Nucl. Phys. B **453**, 334 (1995); The authors of these predictions have verified that their calculated cross sections are consistent over the range of photon transverse energies measured here.
[12] G.D. Lafferty and T.R. Wyatt, Nucl. Instrum. Methods Phys. Res. A **355**, 541 (1995).
[13] C. Avila *et al.* (E811 Collaboration), Phys. Lett. B **445**, 419 (1999); B. Abbott *et al.* (DØ Collaboration), Phys. Rev. D **61**, 072001 (2000).